

ReLaX: Reasoning with Latent Exploration for Large Reasoning Models

Shimin Zhang^{1*} Xianwei Chen^{1*} Yufan Shen^{2*} Ziyuan Ye¹ Jibin Wu^{1†}
¹Hong Kong Polytechnic University ²Shanghai Artificial Intelligence Laboratory

* Equal contribution † Corresponding author: jibin.wu@polyu.edu.hk

Abstract

*Reinforcement Learning with Verifiable Rewards (RLVR) has recently demonstrated remarkable potential in enhancing the reasoning capability of Large Reasoning Models (LRMs). However, RLVR often drives the policy toward over-determinism, resulting in ineffective exploration and premature policy convergence. While promoting token-level diversity has shown promise in mitigating entropy collapse, we argue that the latent dynamics underlying token generation encode a far richer computational structure for steering policy optimization toward a more effective exploration–exploitation tradeoff. To enable tractable analysis and intervention of the latent dynamics of LRMs, we leverage Koopman operator theory to obtain a linearized representation of their hidden state dynamics. This enables us to introduce **Dynamic Spectral Dispersion (DSD)**, a new metric to quantify the heterogeneity of the model’s latent dynamics, serving as a direct indicator of policy exploration. Building upon these foundations, we propose **Reasoning with Latent eXploration (ReLaX)**, a framework that explicitly incorporates latent dynamics to regulate exploration and exploitation during policy optimization. Comprehensive experiments across a wide range of multimodal and text-only reasoning benchmarks show that ReLaX consistently incentivizes reasoning capability and outperforms existing token-level methods. Our project is available at <https://github.com/ZhangShimin1/ReLaX>.*

1. Introduction

Scalable and verifiable reasoning stands as the foundational capability separating current foundation models from artificial general intelligence. Recent progress [9, 13, 18, 30] in RLVR has emerged as an effective paradigm for enhancing the capability of Large Language Models (LLMs) and Multimodal LLMs (MLLMs) on complex reasoning tasks. Whereas, without explicit intervention, reinforcement learning (RL) progressively concentrates the policy distribution and reduces entropy, confining the policy gra-

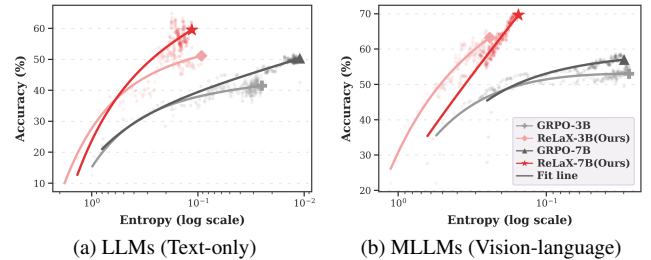


Figure 1. Empirical relationship between policy performance \mathcal{R} and token-level entropy H during RLVR training with (a) text-only LLMs and (b) vision-language models (VLMs). Each scatter training step, the solid curve fitted by $\mathcal{R} = -a \cdot \exp(H) + b$ [10].

dient within a narrow subspace [1, 33]. The sparse reward in RLVR further exacerbates this *entropy collapse* problem, causing the policy to over-exploit prematurely, thereby inhibiting adequate exploration and ultimately leading to suboptimal performance. This bottleneck is supported by empirical evidence from Group Relative Policy Optimization (GRPO) [32, 54], which reveals an exponential relationship between policy entropy H and reward \mathcal{R} : $\mathcal{R} = -a \cdot \exp(H) + b$ [10] (see grey lines in Figure 1). To date, the community has widely recognized the exploration–exploitation tradeoff [36] as the fundamental challenge in scaling RL to achieve improved reasoning performance [11, 16, 22, 40, 45, 53].

Existing endeavors (with a review in the Supplementary Material) mainly focus on raising token-level entropy, including reshaping the reward [6, 7, 16], redesigning policy objectives with entropy-based regularization [20, 50], and heuristically anchoring salient tokens to locally elevate the stochasticity [10, 26, 39, 43, 49, 51, 58]. Despite recent progress, the objective of maintaining higher token-level entropy inherently conflicts with the tendency of RL, which naturally gravitates toward deterministic, low-entropy policies. Moreover, mainstream MLLMs [2, 42, 47] exhibit a pronounced misalignment between cross-modal internal computations and unimodal, text-centric outputs, making it

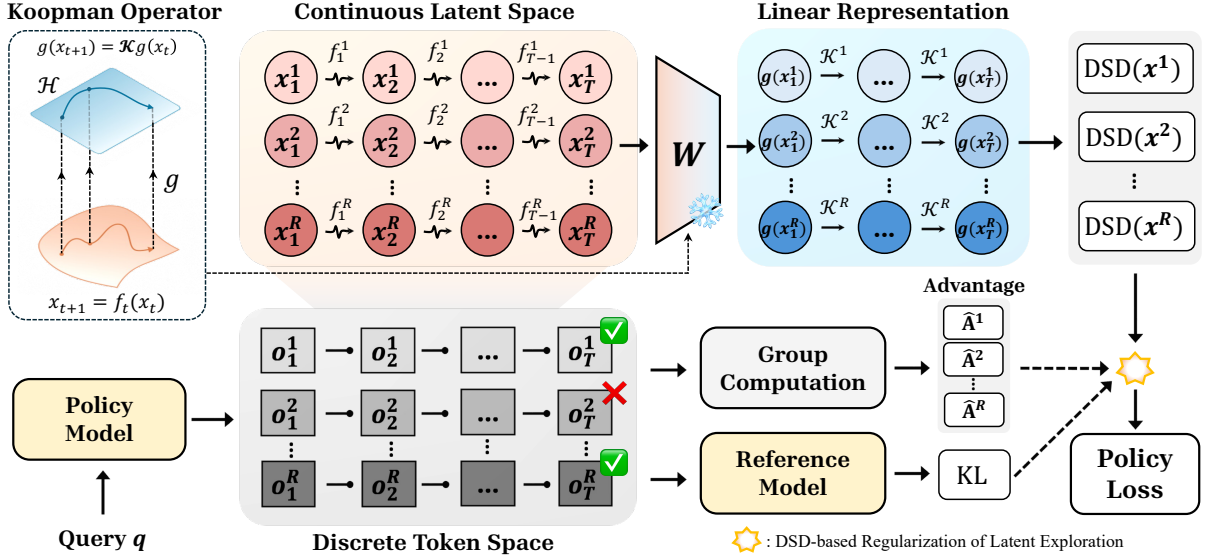


Figure 2. **Overview of ReLaX.** Grounded in Koopman operator theory (upper left), ReLaX employs a neural Koopman dictionary (frozen after one step of learning) during policy optimization to linearize the latent dynamics of last-layer hidden states. This transformation allows us to assess the flexibility of policy’s internal computations through the proposed DSD. The DSD score for each trajectory is subsequently integrated into the GRPO objective, mitigating computational rigidity and enabling a more effective exploration–exploitation tradeoff.

difficult for token-level feedback to accurately reflect the underlying multimodal processing [35, 46]. Taken together, these factors render existing methods inefficient and limit their generalizability when applied to MLLMs.

In this paper, we argue that entropy collapse is the superficial symptom of a deeper pathology: under RLVR, the internal computations that govern token generation gradually lose flexibility and converge into overly rigid patterns. These computations are instantiated through the high-dimensional latent dynamics of hidden states that embed far richer and more stable inductive biases than what is observable in the discrete and sensitive token space. The key to harnessing the continuous latent dynamic of LRMs lies in finding an appropriate representation to make it analytically tractable. Modern Koopman operator theory [3] provides a powerful framework to represent the nonlinear dynamics of a model as linear evolution in an infinite-dimensional space of observables, with the Koopman dictionary governing the functional coordinates of this representation. Building upon this foundation, we introduce a novel metric, **Dynamic Spectral Dispersion (DSD)**, to characterize the flexibility of internal computations in LRMs by quantifying the degree of heterogeneity exhibited in their underlying latent dynamics. We then propose a latent dynamics aware framework for RLVR, **ReLaX (Reasoning with Latent eXploration)**, that employs DSD-based regularization to counteract the rigid internal computation and facilitate effective exploration-exploitation tradeoff. Our main contributions are summarized as follows:

- We propose DSD, a metric that captures the heterogeneity of latent reasoning dynamics in LRMs, providing a more fundamental characterization of policy exploration by probing the model’s internal computational processes rather than its surface-level token statistics.
- Incorporating DSD into the objective of policy optimization, we introduce a novel framework, ReLaX, to effectively facilitate the exploration–exploitation tradeoff and mitigate the performance saturation of RLVR (see Figure 1).
- Extensive experiments demonstrate that ReLaX substantially advances LRM capabilities, outperforming token-level methods and setting new state-of-the-art results on 7 multimodal and 6 text-only reasoning benchmarks. These findings indicate that ReLaX opens a promising direction for advancing reasoning capabilities by transcending token-space interventions and guiding exploration within the more expressive and computationally meaningful latent space.

2. Preliminary

2.1. Problem Formulation

The fine-tuning of foundation models for reasoning tasks can be formulated as a reinforcement learning problem driven by *verifiable rewards*. Let $\pi_\theta(o|q)$ denote the policy model parameterized by θ , which generates a reasoning trajectory $o = (o_0, o_1, \dots, o_T)$ conditioned on a prompt $q \sim \mathcal{D}$, where \mathcal{D} denotes the distribution of input prompts.

The trajectory length is constrained by a maximum context length limit $T \leq L_{\max}$.

Each generated trajectory o is evaluated by a *verifier* that produces a scalar-valued reward(q, o). The verifier provides an objective and automatically checkable signal (e.g., correctness of a mathematical derivation or successful code execution), thus avoiding subjective biases and reward hacking issues in preference-based RL. The training objective of RLVR is to maximize the expected reward under the policy distribution:

$$\max_{\theta} \mathcal{J}(\theta) = \mathbb{E}_{q \sim \mathcal{D}, o \sim \pi_{\theta}(\cdot | q)} [\text{reward}(q, o)], \quad (1)$$

subject to $|o| \leq L_{\max}$.

2.2. Group Relative Policy Optimization

To efficiently optimize the RLVR objective, GRPO serves as a group-based variant of PPO, stabilizing policy improvement by normalizing rewards within each prompt group. For each prompt q , GRPO samples a group of R responses $\{o^i\}_{i=1}^R$ and estimates a group-relative advantage for each trajectory:

$$\hat{A}^i = \frac{\text{reward}(q, o^i) - \text{mean}[\text{reward}(q, \{o^i\}_{i=1}^R)]}{\text{std}[\text{reward}(q, \{o^i\}_{i=1}^R)]}. \quad (2)$$

To handle off-policy data and constrain the optimization step, GRPO adopts the PPO-style clipped surrogate objective:

$$\begin{aligned} \mathcal{J}_{\text{GRPO}}(\theta) &= \mathbb{E}_{q \sim \mathcal{D}, \{o^i\}_{i=1}^R \sim \pi_{\theta_{\text{old}}}(\cdot | q)} \\ &\left[\frac{1}{R} \sum_{i=1}^R \min \left(\frac{\pi_{\theta}(o^i | q)}{\pi_{\theta_{\text{old}}}(o^i | q)} A^i, \right. \right. \\ &\left. \left. \text{clip} \left(\frac{\pi_{\theta}(o^i | q)}{\pi_{\theta_{\text{old}}}(o^i | q)}, 1 - \epsilon, 1 + \epsilon \right) A^i \right) \right]. \end{aligned} \quad (3)$$

To constrain policy updates and ensure stability, a KL-divergence regularization $\mathcal{L}_{\text{KL}} = D_{\text{KL}}(\pi_{\theta} \| \pi_{\text{ref}})$ scaled by β is optionally applied to penalize large deviations from the initial policy. By leveraging group-relative normalization, GRPO provides a stable and scale-invariant learning signal, effectively reducing variance and improving sample efficiency in reasoning-oriented policy updates.

2.3. Koopman Operator Theory and Dynamic Mode Decomposition

The Koopman operator provides a rigorous framework for representing a nonlinear dynamical system within an infinite-dimensional Hilbert space \mathcal{H} . For a discrete-time system governed by $x_{t+1} = f_t(x_t)$, the Koopman operator \mathcal{K} acts on observables $g \in \mathcal{H}$ (Koopman dictionary) as:

$$[\mathcal{K}g](x_t) := g(f_t(x_t)) = g(x_{t+1}). \quad (4)$$

Building upon Koopman operator theory, the Dynamic Mode Decomposition (DMD) [31] serves as a data-driven finite-dimensional approximation of \mathcal{K} . Consider a trajectory with consecutive states $\mathcal{V} = \{g(x_0), g(x_1) \dots, g(x_{t-1})\}$ and their successors $\mathcal{V}^+ = \{g(x_1), g(x_2) \dots, g(x_t)\}$, \mathcal{K} can be estimated by solving a least-squares problem:

$$\mathcal{K} = \arg \min_{\mathcal{K}} \|\mathcal{V}^+ - \mathcal{K}\mathcal{V}\|_F^2 = \mathcal{V}^+ \mathcal{V}^\dagger, \quad (5)$$

where \mathcal{V}^\dagger denotes the pseudoinverse of \mathcal{V} .

Spectral analysis on \mathcal{K} through its eigenvalues enables the characterization of underlying nonlinear dynamics. However, the discretization in DMD often introduces spurious eigenvalues when applied to complex systems with rich continuous spectra, leading to the loss of critical dynamical modes [25, 44]. Recent theoretical advances, particularly ResDMD [8], address this challenge by filtering out poorly convergent spectral components, thereby enabling a more accurate and reliable characterization of complex dynamics. This approach has also shown promise for analyzing the hidden state dynamics of LLMs [57].

3. Proposed Methodology

This section gives a comprehensive presentation of the proposed ReLaX. First, building on Koopman operator theory, Sec. 3.1 introduces DSD as a principled metric for capturing the heterogeneity of latent dynamics (Fig. 2, upper). Second, Sec. 3.2 describes how we construct a reliable and accurate linear representation to support calculating DSD for LRMs. Finally, Sec. 3.3 details how DSD is incorporated into GRPO to achieve an effective exploration-exploitation tradeoff (Fig. 2, lower right).

3.1. Dynamic Spectral Dispersion (DSD)

The explicit Chain-of-Thought (CoT) in LRMs is decoded from latent hidden representations evolving under:

$$x_t = \mathcal{F}(x_{t-1}, \omega_t), \quad \omega_t \sim \mathcal{P}_{\omega}, \quad (6)$$

where \mathcal{F} defines a stochastic nonlinear dynamical system over the latent state space. The stochasticity ω_t (e.g., temperature, top- p , and top- k sampling) not only determines the decoded CoT, but also injects perturbations into the latent trajectory. The extent to which these perturbations induce effective exploration depends on the richness of the intrinsic hidden state dynamics, which determines whether stochastic inputs can be translated into diverse latent trajectories.

However, the nonlinear and high-dimensional nature of latent dynamics presents substantial challenges for effectively and accurately capturing their underlying dynamics.

The Koopman operator offers a rigorous framework for analyzing nonlinear dynamics by embedding the latent dynamics into an infinite-dimensional function space, where their evolution is governed by a linear operator \mathcal{K} . The spectral decomposition of \mathcal{K} reveals fundamental dynamical modes (e.g., growth, decay, and oscillation) that govern the structure of the resulting reasoning trajectories. Therefore, the distribution of spectral modes characterizes the intrinsic structure of the underlying dynamics: a concentrated spectrum implies degenerate, repetitive behavior, whereas a dispersed spectrum signifies a richer and more expressive dynamical system.

Leveraging this insight, we put forward DSD as an operational proxy for the policy model’s computational flexibility. Formally, given a sequence of hidden states $x \in \mathbb{R}^{T \times d}$ and its approximated Koopman operator \mathcal{K} , the DSD is defined as the variance of the Koopman eigenvalue magnitudes:

$$\text{DSD}(x) = \text{Var}(|\Lambda|), \text{ where } \mathcal{K}\Phi = \Phi\Lambda. \quad (7)$$

Higher DSD scores correspond to richer intrinsic dynamical spectra, indicating that the model avoids collapsing into rigid computational patterns. This dynamical flexibility enables stochastic perturbations to be effectively leveraged, giving rise to diverse latent trajectories that support sustained and efficient exploration during policy optimization. The evolution of latent trajectory in a low-dimensional space is visualized in the Supplementary Material.

3.2. Koopman Dictionary Learning

A core challenge in applying the Koopman operator is selecting an appropriate function space in which the operator \mathcal{K} can faithfully linearize the policy model’s latent dynamics—an especially difficult problem given the high dimensionality and strong nonlinearity of LRMs. To address this, we adopt ResKoopNet [48], an extension of ResDMD that learns a neural Koopman dictionary. This enables a more accurate and numerically stable approximation of the Koopman operator and its spectrum, which is essential for reliable DSD computation.

Specifically, the Koopman observables g are parameterized by a single linear layer W followed by a sigmoid activation $\sigma(\cdot)$:

$$g(x) = \sigma(Wx), \quad W \in \mathbb{R}^{d \times m}, \quad (8)$$

where m represents the dimensionality of the approximated Koopman operator. The dictionary W is optimized using latent trajectories $\{x_i\}_{i=1}^{B \times R}$ collected from the last hidden-layer of initial policy, where B denotes the policy training batch size. The optimization objective for W is to minimize the spectral residual of the Koopman operator:

$$W = \arg \min \frac{1}{BR} \left\| (\mathcal{V}^+ - \mathcal{K}\mathcal{V})\Phi \right\|_F^2, \quad (9)$$

where Φ denotes the eigenvectors of \mathcal{K} . Once optimized, W is frozen during subsequent policy training to ensure a consistent function space for portraying policy latent dynamics throughout optimization. A more detailed presentation related to Koopman dictionary learning is provided in the Supplementary Material.

3.3. ReLaX

DSD characterizes the policy exploration from a computational perspective and supports gradient propagation, providing a principled basis for steering policy optimization toward an effective exploration–exploitation tradeoff. Formally, for hidden states $\{x^i\}_{i=1}^R$ correspond to group responses $\{o^i\}_{i=1}^R$, we define a sequence-level regularization term \mathcal{L}_{xp} associated with the corresponding DSD scores as:

$$\mathcal{L}_{\text{xp}} = \log \left(\frac{1}{R} \sum_{i=1}^R \exp(-\text{DSD}(x^i)) \right), \quad (10)$$

where the log-mean-exp computation smooths DSD numerically, enhancing gradient stability during optimization.

While this regularization alleviates computational rigidity by discouraging the latent dynamics from converging to a homogeneous mode, excessive exploration can undermine the necessary exploitation. Accordingly, ReLaX integrates two control mechanisms to maintain latent exploration at an appropriate operating level. First, to ensure that exploration occurs within a meaningful subspace of the latent dynamics, we weight the DSD scores by the advantages truncated to their positive part. This design constrains the policy model to become more flexible only along trajectories that yield positive reward, preventing uninformative or detrimental exploration. The resulting advantage-shaped regularization is expressed as:

$$\tilde{\mathcal{L}}_{\text{xp}} = \log \left(\frac{1}{R} \sum_{i=1}^R \exp(-\text{clip}(\hat{A}^i, 0) \cdot \text{DSD}(x^i)) \right). \quad (11)$$

Nevertheless, an over-dispersion of dynamic spectral modes within positive trajectories still induces instability. KL regularization acts as an elastic constraint to stabilize training, albeit at the cost of slower convergence [10, 49, 51, 58]. We compromise by applying an adaptive KL regularization to softly constrain policy updates for trajectories that exhibit excessive dynamic divergence, while allowing those with remaining exploration potential to proceed freely. The overall objective of ReLaX is thus formulated as:

$$\mathcal{J}(\theta) = \mathcal{J}_{\text{GRPO}}(\theta) + \alpha \tilde{\mathcal{L}}_{\text{xp}} + \beta \sum_i^{\mathcal{I}} D_{\text{KL}}(\pi_\theta(o^i) \parallel \pi_{\text{ref}}(o^i)), \quad (12)$$

where α controls the strength of regularization for latent exploration, and $\mathcal{I} = \{i \mid \text{DSD}(x^i) > \xi\}$ denotes the subset of trajectories whose DSD scores exceed a threshold ξ ,

thereby requiring KL penalization. A complete pseudocode of ReLaX is included in the Supplementary Material.

4. Experiments

To establish the effectiveness of ReLaX, we perform extensive experiments on both VLMs and LLMs at the 3B and 7B scales. We begin in Section 4.1 by outlining some important experimental setups. Section 4.2 then reports results on a broad suite of multimodal and text-only mathematical reasoning benchmarks, comparing ReLaX against state-of-the-art LRMs. Section 4.3 presents an ablation study illustrating the role of each component in ReLaX. Finally, beyond the benchmarking results, Section 4.4 offers a comprehensive comparison with previous work that focus on token space.

4.1. Experimental Settings

We conduct experiments on both VLMs and LLMs within the GRPO framework, which is widely adopted in recent studies on the emergence of LRMs. Below, we outline the key experimental configurations used in our experiments:

4.1.1. Training Data and Benchmarks

VLMs are trained on the ViRL39K dataset from [38], which contains 38,870 curated and verifiable multimodal question-answer pairs. We adjust the query special tokens to align with our implementation framework. To comprehensively evaluate multimodal reasoning performance, 7 challenging multimodal reasoning benchmarks are involved, including multidisciplinary datasets (MMM U [52], MM-Star [4], EMMA [14]) and mathematical datasets (MathVista [27], MathVerse [56], MathVision [41], and DynaMath [59]). We report the mean@1 accuracy using greedy decoding.

For LLMs training, we construct a merged dataset by combining the DAPO-Math-17K corpus [51] with the Level 3–5 subsets of the MATH training set [15], yielding approximately 22K mathematical queries with a broader range of difficulty. For evaluation, we use MATH500 (500 random samples from the MATH test set), Minerva [21], AMC 2022 & 2023 [29], and AIME 2024 & 2025 [24]. We report mean@1 on MATH500 and Minerva, and mean@32 on AMC and AIME for robust evaluation due to the limited size of these test sets.

4.1.2. Baselines and Implementations

The multimodal baselines include MM-Eureka [28], Vision-R1 [17], R1-VL [55], OpenVLThinker [12], VL-Rethinker [38], and SRPO [19]. For text-only mathematical reasoning, we benchmark ReLaX against a set of recent RLVR algorithms, including SimpleRL [54], DAPO [49], KL-Cov [10], R1-zero-Div [50], and FR3E [58]. Our method is implemented on the VeRL codebase [34]. Additional details on baselines, training hyperparameters, evalu-

ation settings, and our ReLaX implementation are provided in the Supplementary Material.

4.2. Main Results

4.2.1. Multimodal Reasoning

For multimodal experiments, we adopt Qwen2.5-VL-Instruct as the base model. As shown in Table 1, ReLaX-VL-3B and ReLaX-VL-7B yield absolute improvements of 8.3 and 5.3 in average mean@1 accuracy across 7 multimodal benchmarks, respectively, over their corresponding base models. Notably, ReLaX-VL-7B achieves an average score of 53.2, establishing a new state-of-the-art among existing 7B scale multimodal reasoning models and surpassing the previous best, VL-Rethinker-7B (52.5). At the 3B scale, ReLaX-VL-3B also shows strong competitiveness, outperforming several previous 7B-level models, including R1-VL (40.9) and OpenVLThinker (45.3).

The training dynamics shown in Fig. 3 further highlight how ReLaX enhances the capability of multimodal LRMs. Under vanilla GRPO (gray), both policy entropy and DSD exhibit a rapid decline within the first 50 steps. This indicates that the model quickly collapses into a rigid pattern—both in its internal latent dynamics and output tokens—ultimately leading to stagnant policy improvement due to reduced flexibility. In contrast, ReLaX maintains substantially more diverse latent dynamics and stabilizes the entropy at a higher yet well-regulated level. This balanced behavior enables the policy to continue improving and ultimately achieves a relative performance gain of 10% on both the 3B and 7B models. These results demonstrate that ReLaX unlocks a substantial amount of previously untapped potential by explicitly facilitating the exploration-exploitation tradeoff during RLVR—an aspect that prior MLLM work has largely overlooked.

4.2.2. Text-only Mathematical Reasoning

For text-only reasoning, we conduct experiments on three base models: Qwen2.5-3B-Base, Qwen2.5-7B-Base, and Qwen2.5-7B-Math. We compare ReLaX against existing RLVR algorithms, including the GRPO baseline (referred to as SimpleRL [54] for 7B-scale models) and several variants designed to promote the policy exploration at token space. As shown in Table 2, ReLaX achieves substantial improvements over all three base models as well as their vanilla GRPO counterparts. Moreover, ReLaX outperforms existing GRPO variants across 6 mathematical reasoning benchmarks. In particular, ReLaX surpasses the previous state-of-the-art publicly available baseline, FR3E [58], by 4.3 on Qwen2.5-7B-Base and 6.3 on Qwen2.5-7B-Math. The training dynamics in text-only experiments on Qwen2.5-Base with 3B and 7B scales can be found in Supplementary Material. To showcase that ReLaX generalizes across model families, we additionally evaluate it on Llama3.2-

Model	MathVista <i>testmini</i>	MathVerse <i>testmini</i>	MathVision <i>test</i>	DynaMath <i>overall</i>	MMMU <i>val</i>	MMStar <i>overall</i>	EMMA <i>overall</i>	Average
General Multimodal LLMs								
Qwen2-VL-7B [42]	58.2	19.7	16.3	42.1	54.1	60.7	20.2	38.8
Qwen2.5-VL-3B [2]	62.3	33.5 [†]	21.2	40.0 [†]	46.3	55.9	19.2 [†]	39.8
Qwen2.5-VL-7B [2]	68.2	49.2	25.1	53.2	54.3	63.9	21.5	47.9
Qwen2.5-VL-72B [2]	74.8	57.6	38.1	-	70.2	70.8	-	-
Intern2-VL-8B [5]	58.3	22.8	17.4	39.7	51.2	61.5	19.8	38.7
Intern2.5-VL-8B [5]	64.4	39.5	19.7	-	56.0	-	20.6	-
Llava-OV-7B [23]	63.2	26.2	18.5	-	48.8	-	18.3	-
Kimi-VL-16B [37]	68.7	44.9	21.4	-	55.7	-	-	-
Reasoning Multimodal LLMs								
MM-Eureka-7B [28]	73.0	50.3	26.9	54.4 [†]	55.2	64.3 [†]	23.5	49.7
MM-Eureka-8B [28]	67.1	40.4	22.2	-	49.2	-	21.5	-
Vision-R1-7B [17]	73.5	52.4	27.2	52.0 [†]	54.7	60.9 [†]	22.4	49.0
R1-VL-7B [55]	63.5	40.0	24.7	45.2	44.5	60.0	8.3	40.9
OpenVLThinker-7B [12]	70.2	47.9	25.3	38.6 [†]	52.5	56.3 [†]	26.6	45.3
VL-Rethinker-7B [38]	74.9	54.2	32.3	55.2 [†]	56.7	64.2 [†]	29.7	52.5
SRPO-7B [19]	75.8	55.8	32.9	-	57.1	-	29.6	-
ReLaX-VL-3B (Ours)	70.7	46.2	27.6	52.2	52.2	60.7	26.9	48.1
ReLaX-VL-7B (Ours)	77.1	55.7	30.2	55.9	57.4	65.5	30.6	53.2

Table 1. Comparison of VLM performance (mean@1 accuracy) across multiple multimodal reasoning benchmarks. For 7B scale LRMs, the top-performing and runner-up results of VLMs within each column are marked in red and blue, respectively. [†] indicates our reproduced results using publicly available models and standard evaluation code. “-” denotes missing results due to unavailable models.

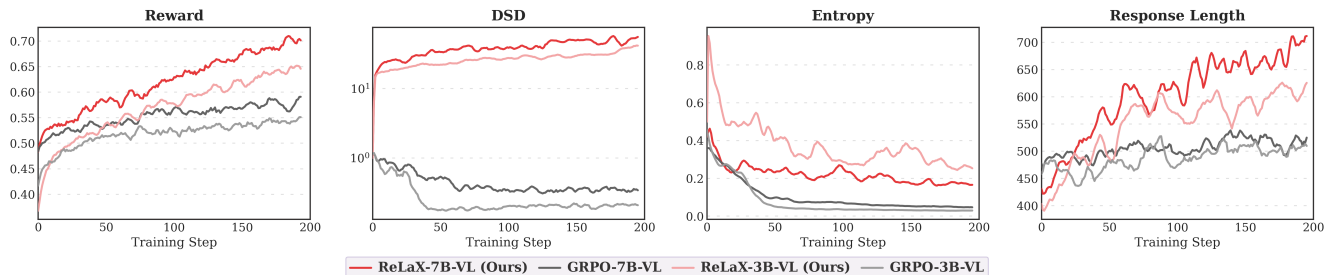


Figure 3. Comparison of training dynamics for *Reward*, *DSD*, *Entropy*, and *Response Length* under ReLaX (red) and vanilla GRPO (gray) on Qwen2.5-VL-Instruct at the 3B and 7B scales.

3B-Instruct and Qwen3-4B. The corresponding results are provided in the Supplementary Material.

4.3. Ablation Study

We perform ablation studies to analyze the DSD-based regularization in ReLaX from two perspectives.

Hyperparameters Sensitivity. We first evaluate the impact of the DSD-based regularization coefficient α , which governs the strength of encouraging the policy to explore more diverse latent dynamics. As shown in Fig. 4, increasing this coefficient leads to a pronounced rise in policy entropy, in-

dicating that nudging the model away from rigid internal computation regimes effectively mitigates entropy collapse. However, higher entropy does not necessarily translate into better policy convergence. We observe that ReLaX achieves the highest policy reward when the coefficient is set to 0.1. A coefficient of 0.3 yields only a marginal improvement over vanilla GRPO, while an overly strong coefficient (e.g., 1.0) harms performance. Additional results on Koopman dimension m and DSD threshold ξ are provided in the Supplementary Material.

Adaptive KL Regularization & Advantage Shaping. To

Model	Size	MATH500	Minerva	AMC22	AMC23	AIME24	AIME25	Average
		Mean@1	Mean@1	Mean@32	Mean@32	Mean@32	Mean@32	
Qwen2.5-base	3B	18.4	2.6	12.5 [†]	7.0	0.6	0.3	5.9
+Vanilla GRPO[32]	3B	69.2	23.5 [†]	25.9 [†]	51.6	7.5	4.5	26.0
+DCPO[49]	3B	71.2	-	-	55.8	7.5	4.7	-
+ReLaX (Ours)	3B	71.6	26.1	44.8	63.5	8.8	6.2	31.6
Qwen2.5-base	7B	64.6	5.7	21.4 [†]	30.0	0.3	0.1	17.4
+SimpleRL[54]	7B	78.2	38.6	39.5 [†]	62.5	15.6	8.9 [†]	34.8
+DAPO[51]	7B	77.8	35.3	-	60.0	18.1	11.5	-
+KL-Cov[10]	7B	80.8	38.2	-	61.4	22.6	12.9	-
+HICRA[39]	7B	80.2	38.6	-	55.1	18.8	14.8	-
+FR3E[58]	7B	79.0	39.0	49.2 [†]	67.5	25.2	14.8 [†]	39.2
+ReLaX (Ours)	7B	82.4	39.1	65.4	84.1	19.7	13.8	43.5
Qwen2.5-Math-base	7B	52.4	10.7	25.4 [†]	52.2	16.6	6.3	23.4
+SimpleRL[54]	7B	77.4	32.0	57.0 [†]	60.8	26.7	9.3	37.6
+DAPO[51]	7B	81.6	38.2	-	62.5	31.6	14.9	-
+DCPO[49]	7B	82.5	-	-	79.8	38.8	17.2	-
+R1-zero-Div[50]	7B	77.2	31.6 [†]	50.2 [†]	58.0 [†]	17.5 [†]	10.0 [†]	34.9
+FR3E[58]	7B	82.2	40.8	64.1 [†]	67.5	26.7	18.1 [†]	42.8
+ReLaX (Ours)	7B	85.6	43.4	71.9	88.9	36.9	17.3	49.1

Table 2. Comparison of LLM performance (mean@1 & mean@32) across multiple text-only mathematical reasoning benchmarks. For each base model, the top-performing and runner-up results of RLVR algorithms within each column are marked in red and blue, respectively. [†] indicates our reproduced results using publicly available models and standard evaluation code. “-” denotes missing results due to unavailable models.

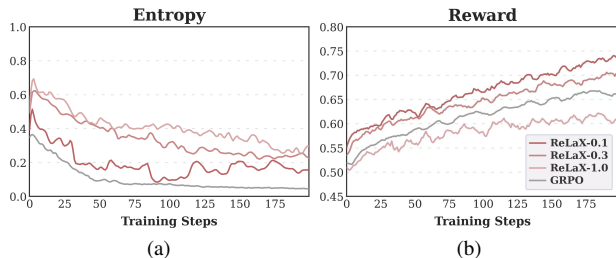


Figure 4. Training dynamics of policy entropy and reward on 3B scale Qwen2.5-VL-3B models by ReLaX with different DSD-based regularization coefficients (1.0, 0.3, 0.1, 0).

stabilize policy optimization, ReLaX incorporates adaptive KL regularization and advantage shaping. We evaluate their contributions via ablations on Qwen2.5-7B-Math across six mathematical reasoning benchmarks. As shown in Fig. 5, removing adaptive KL regularization applies uniform penalties across trajectories regardless of their DSD scores, leading to consistently degraded performance, consistent with prior findings [10, 51]. In contrast, ReLaX penalizes only trajectories with overly dispersed dynamics. Removing advantage shaping causes a more severe drop:

exploration becomes indiscriminate in latent space, including directions with negative or uninformative rewards, resulting in training collapse and even worse performance than the base model.

Overall, these results suggest that ReLaX achieves a balance between exploration and exploitation through a principled choice of hyperparameters and beneficial trajectory selection, enabling controlled, conditional latent exploration while maintaining stable learning.

4.4. Comparative Analysis

ReLaX operates beyond token-level manipulation by reshaping intrinsic latent reasoning dynamics. While it demonstrates clear performance gains on text-only reasoning benchmarks (Table 2), its advantages over token-level methods in multimodal reasoning, as well as its impact on specific reasoning behaviors, remain unclear. We therefore compare it with representative token-level methods in this section through multimodal generalization and qualitative analysis.

4.4.1. Multimodal Generalization

We evaluate ReLaX against entropy regularization [50] and KL-Cov [10] on Qwen2.5-VL-3B. As shown in Fig. 6, Re-

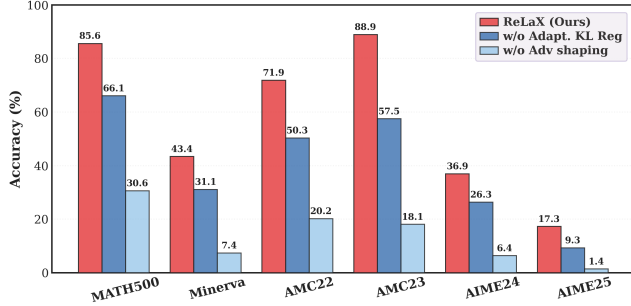


Figure 5. Evaluation results from the ablation study on Qwen2.5-7B-Math for text-only reasoning tasks. Results by full ReLaX is highlighted in red, while the dark-blue and light-blue bars respectively correspond to its ablations without adaptive KL regularization and advantage shaping.

LaX consistently outperforms both methods across multimodal benchmarks. Naively extending entropy regularization to multimodal training increases both DSD and token-level entropy, but at the cost of semantic drift that degrade performance. While KL-Cov provides modest gains over vanilla GRPO, it does not prevent the rigidification of latent dynamics, suggesting that promoting token-level exploration have limited influence on the latent space where cross-modal computation takes place. Interestingly, KL-Cov performs relatively better on multimodal mathematics benchmarks such as MathVista, MathVerse, and MathVision (full results in the Supplementary Material), where visual grounding is less critical. In contrast, ReLaX achieves substantially larger gains on more visually grounded tasks (e.g., +7.7 on EMMA-Physics).

These findings indicate that explicitly encouraging flexible latent reasoning dynamics is more appropriate for MLLMs, as it facilitates a more effective exploration–exploitation trade-off and leads to better generalization in multimodal reasoning.

4.4.2. Qualitative Results

We further present qualitative case studies to examine reasoning behaviors underlying the benchmark results. We first analyze a mathematic query from AMC23 [29], comparing the models trained with ReLaX and entropy regularization (R1-zero-Div [50]) from Qwen2.5-7B-Math. As shown in Supplementary Material Tab. 7, both models produce the correct final answer and attempt *self-verification*. However, ReLaX-7B performs meaningful validation by invoking relevant mathematical principles, whereas R1-zero-Div generates Python code for verification—an ineffective strategy given the lack of code execution. This behavior suggests that simply encouraging uncertainty on token generation may lead to hallucinated or inefficient reasoning. Additionally for VLMs, We compare ReLaX with KL-Cov on the Qwen2.5-VL-3B model using a sample from the Dy-

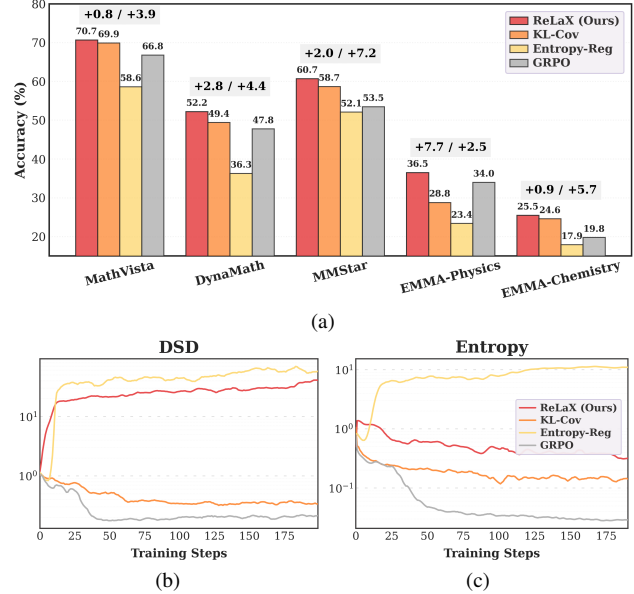


Figure 6. Comparison of RLVR training methods on Qwen2.5-3B-VL. (a) Evaluation results across 5 multimodal reasoning benchmarks. The values above each bar denote ReLaX’s performance gains over KL-Cov (left) and vanilla GRPO (right). (b) and (c) Training dynamics of policy DSD and policy entropy, respectively.

naMath dataset [59], which evaluates reasoning robustness by testing whether models remain consistent across variants of the same question (e.g., modified numerical values or visual details). As shown in Supplementary Material Tab. 8, ReLaX demonstrates consistent visual understanding across all variants, yielding correct answers. In contrast, KL-Cov fails on several variants due to misinterpretation of visual cues or incorrect reasoning, indicating degraded visual comprehension and reasoning capability. An additional case of this perspective from MMMU [52] is included in the Supplementary Material Tab. 9.

5. Conclusion

In this work, we introduced ReLaX, a new RLVR training paradigm that explicitly promotes heterogeneity in latent dynamics during policy optimization. By facilitating more flexible internal computations for LRMs, ReLaX effectively mitigates the performance saturation induced by mode collapse in RLVR. Extensive evaluations across multiple benchmarks show that ReLaX consistently improves reasoning capability under RLVR paradigm across diverse model families, outperforming existing methods that focus on token-level diversity. These results indicate that steering exploration via latent dynamics offers a more principled solution to the exploration–exploitation trade-off, and point to latent space as a powerful and scalable frontier for advancing LRM capabilities.

References

- [1] Alekh Agarwal, Sham M Kakade, Jason D Lee, and Gaurav Mahajan. On the theory of policy gradient methods: Optimality, approximation, and distribution shift. *Journal of Machine Learning Research*, 22(98):1–76, 2021. 1
- [2] Shuai Bai, Keqin Chen, Xuejing Liu, Jialin Wang, Wenbin Ge, Sibao Song, Kai Dang, Peng Wang, Shijie Wang, Jun Tang, et al. Qwen2. 5-vl technical report. *arXiv preprint arXiv:2502.13923*, 2025. 1, 6
- [3] Steven L Brunton, Marko Budišić, Eurika Kaiser, and J Nathan Kutz. Modern koopman theory for dynamical systems. *arXiv preprint arXiv:2102.12086*, 2021. 2
- [4] Lin Chen, Jinsong Li, Xiaoyi Dong, Pan Zhang, Yuhang Zang, Zehui Chen, Haodong Duan, Jiaqi Wang, Yu Qiao, Dahua Lin, and Feng Zhao. Are we on the right way for evaluating large vision-language models? In *The Thirty-eighth Annual Conference on Neural Information Processing Systems*, 2024. 5
- [5] Zhe Chen, Weiyun Wang, Yue Cao, Yangzhou Liu, Zhangwei Gao, Erfei Cui, Jinguo Zhu, Shenglong Ye, Hao Tian, Zhaoyang Liu, et al. Expanding performance boundaries of open-source multimodal models with model, data, and test-time scaling. *arXiv preprint arXiv:2412.05271*, 2024. 6
- [6] Zhipeng Chen, Xiaobo Qin, Youbin Wu, Yue Ling, Qinghao Ye, Wayne Xin Zhao, and Guang Shi. Pass@k training for adaptively balancing exploration and exploitation of large reasoning models. *arXiv preprint arXiv:2508.10751*, 2025. 1
- [7] Daixuan Cheng, Shaohan Huang, Xuekai Zhu, Bo Dai, Wayne Xin Zhao, Zhenliang Zhang, and Furu Wei. Reasoning with exploration: An entropy perspective. *arXiv preprint arXiv:2506.14758*, 2025. 1
- [8] Matthew J Colbrook and Alex Townsend. Rigorous data-driven computation of spectral properties of koopman operators for dynamical systems. *Communications on Pure and Applied Mathematics*, 77(1):221–283, 2024. 3, 1
- [9] Gheorghe Comanici, Eric Bieber, Mike Schaekermann, Ice Pasupat, Noveen Sachdeva, Inderjit Dhillon, Marcel Blisstein, Ori Ram, Dan Zhang, Evan Rosen, et al. Gemini 2.5: Pushing the frontier with advanced reasoning, multimodality, long context, and next generation agentic capabilities. *arXiv preprint arXiv:2507.06261*, 2025. 1
- [10] Ganqu Cui, Yuchen Zhang, Jiacheng Chen, Lifan Yuan, Zhi Wang, Yuxin Zuo, Haozhan Li, Yuchen Fan, Huayu Chen, Weize Chen, et al. The entropy mechanism of reinforcement learning for reasoning language models. *arXiv preprint arXiv:2505.22617*, 2025. 1, 4, 5, 7
- [11] Jia Deng, Jie Chen, Zhipeng Chen, Wayne Xin Zhao, and Ji-Rong Wen. Decomposing the entropy-performance exchange: The missing keys to unlocking effective reinforcement learning. *arXiv preprint arXiv:2508.02260*, 2025. 1
- [12] Yihe Deng, Hritik Bansal, Fan Yin, Nanyun Peng, Wei Wang, and Kai-Wei Chang. Openvlthinker: Complex vision-language reasoning via iterative sft-rl cycles. In *The Thirtieth Annual Conference on Neural Information Processing Systems*, 2025. 5, 6
- [13] Daya Guo, Dejian Yang, Haowei Zhang, Junxiao Song, Ruoyu Zhang, Runxin Xu, Qihao Zhu, Shirong Ma, Peiyi Wang, Xiao Bi, et al. Deepseek-r1: Incentivizing reasoning capability in llms via reinforcement learning. *arXiv preprint arXiv:2501.12948*, 2025. 1
- [14] Yunzhuo Hao, Jiawei Gu, Huichen Will Wang, Linjie Li, Zhengyuan Yang, Lijuan Wang, and Yu Cheng. Can MLLMs reason in multimodality? EMMA: An enhanced multimodal reasoning benchmark. In *Forty-second International Conference on Machine Learning*, 2025. 5
- [15] Dan Hendrycks, Collin Burns, Saurav Kadavath, Akul Arora, Steven Basart, Eric Tang, Dawn Song, and Jacob Steinhardt. Measuring mathematical problem solving with the math dataset. *arXiv preprint arXiv:2103.03874*, 2021. 5
- [16] Zican Hu, Shilin Zhang, Yafu Li, Jianhao Yan, Xuyang Hu, Leyang Cui, Xiaoye Qu, Chunlin Chen, Yu Cheng, and Zhi Wang. Diversity-incentivized exploration for versatile reasoning. *arXiv preprint arXiv:2509.26209*, 2025. 1
- [17] Wenxuan Huang, Bohan Jia, Zijie Zhai, Shaosheng Cao, Zheyu Ye, Fei Zhao, Zhe Xu, Yao Hu, and Shaohui Lin. Vision-r1: Incentivizing reasoning capability in multimodal large language models. *arXiv preprint arXiv:2503.06749*, 2025. 5, 6
- [18] Aaron Jaech, Adam Kalai, Adam Lerer, Adam Richardson, Ahmed El-Kishky, Aiden Low, Alec Helyar, Aleksander Madry, Alex Beutel, Alex Carney, et al. Openai o1 system card. *arXiv preprint arXiv:2412.16720*, 2024. 1
- [19] Qian Jiang, Changyou Chen, Han Zhao, Liqun Chen, Qing Ping, Son Dinh Tran, Yi Xu, Belinda Zeng, and Trishul Chilimbi. Understanding and constructing latent modality structures in multi-modal representation learning. In *Proceedings of the IEEE/CVF Conference on Computer Vision and Pattern Recognition*, pages 7661–7671, 2023. 5, 6
- [20] Shiye Lei, Zhihao Cheng, Kai Jia, and Dacheng Tao. Revisiting llm reasoning via information bottleneck. *arXiv preprint arXiv:2507.18391*, 2025. 1
- [21] Aitor Lewkowycz, Anders Andreassen, David Dohan, Ethan Dyer, Henryk Michalewski, Vinay Ramasesh, Ambrose Slone, Cem Anil, Imanol Schlag, Theo Gutman-Solo, et al. Solving quantitative reasoning problems with language models. *Advances in neural information processing systems*, 35: 3843–3857, 2022. 5
- [22] Ang Li, Zhihang Yuan, Yang Zhang, Shouda Liu, and Yisen Wang. Know when to explore: Difficulty-aware certainty as a guide for llm reinforcement learning. *arXiv preprint arXiv:2509.00125*, 2025. 1
- [23] Bo Li, Yuanhan Zhang, Dong Guo, Renrui Zhang, Feng Li, Hao Zhang, Kaichen Zhang, Peiyuan Zhang, Yanwei Li, Ziwei Liu, and Chunyuan Li. LLaVA-onevision: Easy visual task transfer. *Transactions on Machine Learning Research*, 2025. 6
- [24] Jia Li, Edward Beeching, Lewis Tunstall, Ben Lipkin, Roman Soletskyi, Shengyi Huang, Kashif Rasul, Longhui Yu, Albert Q Jiang, Ziju Shen, et al. NuminaMath: The largest public dataset in ai4maths with 860k pairs of competition math problems and solutions. *Hugging Face repository*, 13 (9):9, 2024. 5

- [25] Qianxiao Li, Felix Dietrich, Erik M Bollt, and Ioannis G Kevrekidis. Extended dynamic mode decomposition with dictionary learning: A data-driven adaptive spectral decomposition of the koopman operator. *Chaos: An Interdisciplinary Journal of Nonlinear Science*, 27(10), 2017. 3, 1
- [26] Qingbin Li, Rongkun Xue, Jie Wang, Ming Zhou, Zhi Li, Xiaofeng Ji, Yongqi Wang, Miao Liu, Zheming Yang, Minghui Qiu, et al. Cure: Critical-token-guided re-concatenation for entropy-collapse prevention. *arXiv preprint arXiv:2508.11016*, 2025. 1
- [27] Pan Lu, Hritik Bansal, Tony Xia, Jiacheng Liu, Chunyuan Li, Hannaneh Hajishirzi, Hao Cheng, Kai-Wei Chang, Michel Galley, and Jianfeng Gao. Mathvista: Evaluating mathematical reasoning of foundation models in visual contexts. In *The Twelfth International Conference on Learning Representations*, 2024. 5
- [28] Fanqing Meng, Lingxiao Du, Zongkai Liu, Zhixiang Zhou, Quanfeng Lu, Daocheng Fu, Tiancheng Han, Botian Shi, Wenhai Wang, Junjun He, et al. Mm-eureka: Exploring the frontiers of multimodal reasoning with rule-based reinforcement learning. *arXiv preprint arXiv:2503.07365*, 2025. 5, 6
- [29] Long Ouyang, Jeffrey Wu, Xu Jiang, Diogo Almeida, Carroll Wainwright, Pamela Mishkin, Chong Zhang, Sandhini Agarwal, Katarina Slama, Alex Ray, et al. Training language models to follow instructions with human feedback. *Advances in neural information processing systems*, 35:27730–27744, 2022. 5, 8
- [30] Yi Peng, Peiyu Wang, Xiaokun Wang, Yichen Wei, Jiangbo Pei, Weijie Qiu, Ai Jian, Yunzhuo Hao, Jiachun Pan, Tianyidan Xie, et al. Skywork rlv: Pioneering multimodal reasoning with chain-of-thought. *arXiv preprint arXiv:2504.05599*, 2025. 1
- [31] Peter J Schmid. Dynamic mode decomposition and its variants. *Annual Review of Fluid Mechanics*, 54(1):225–254, 2022. 3
- [32] Zhihong Shao, Peiyi Wang, Qihao Zhu, Runxin Xu, Junxiao Song, Xiao Bi, Haowei Zhang, Mingchuan Zhang, YK Li, Yang Wu, et al. Deepseekmath: Pushing the limits of mathematical reasoning in open language models. *arXiv preprint arXiv:2402.03300*, 2024. 1, 7, 6
- [33] Han Shen. On entropy control in llm-rl algorithms. *arXiv preprint arXiv:2509.03493*, 2025. 1
- [34] Guangming Sheng, Chi Zhang, Zilingfeng Ye, Xibin Wu, Wang Zhang, Ru Zhang, Yanghua Peng, Haibin Lin, and Chuan Wu. Hybridflow: A flexible and efficient rlhf framework. *arXiv preprint arXiv: 2409.19256*, 2024. 5, 2
- [35] Quan Sun, Yufeng Cui, Xiaosong Zhang, Fan Zhang, Qiyang Yu, Yueze Wang, Yongming Rao, Jingjing Liu, Tiejun Huang, and Xinlong Wang. Generative multimodal models are in-context learners. In *Proceedings of the IEEE/CVF conference on computer vision and pattern recognition*, pages 14398–14409, 2024. 2
- [36] Richard S Sutton. Learning to predict by the methods of temporal differences. *Machine learning*, 3(1):9–44, 1988. 1
- [37] Kimi Team, Angang Du, Bohong Yin, Bowei Xing, Bowen Qu, Bowen Wang, Cheng Chen, Chenlin Zhang, Chen-zhuang Du, Chu Wei, et al. Kimi-vl technical report. *arXiv preprint arXiv:2504.07491*, 2025. 6
- [38] Haozhe Wang, Chao Qu, Zuming Huang, Wei Chu, Fangzhen Lin, and Wenhui Chen. VL-rethinker: Incentivizing self-reflection of vision-language models with reinforcement learning. In *The Thirty-ninth Annual Conference on Neural Information Processing Systems*, 2025. 5, 6
- [39] Haozhe Wang, Qixin Xu, Che Liu, Junhong Wu, Fangzhen Lin, and Wenhui Chen. Emergent hierarchical reasoning in llms through reinforcement learning. *arXiv preprint arXiv:2509.03646*, 2025. 1, 7, 3, 6
- [40] Jiakang Wang, Runze Liu, Fuzheng Zhang, Xiu Li, and Guorui Zhou. Stabilizing knowledge, promoting reasoning: Dual-token constraints for rlvr. *arXiv preprint arXiv:2507.15778*, 2025. 1
- [41] Ke Wang, Junting Pan, Weikang Shi, Zimu Lu, Houxing Ren, Aojun Zhou, Mingjie Zhan, and Hongsheng Li. Measuring multimodal mathematical reasoning with MATH-vision dataset. In *The Thirty-eight Conference on Neural Information Processing Systems Datasets and Benchmarks Track*, 2024. 5
- [42] Peng Wang, Shuai Bai, Sinan Tan, Shijie Wang, Zhihao Fan, Jinze Bai, Keqin Chen, Xuejing Liu, Jialin Wang, Wenbin Ge, et al. Qwen2-vl: Enhancing vision-language model’s perception of the world at any resolution. *arXiv preprint arXiv:2409.12191*, 2024. 1, 6
- [43] Shenzhi Wang, Le Yu, Chang Gao, Chujie Zheng, Shixuan Liu, Rui Lu, Kai Dang, Xionghui Chen, Jianxin Yang, Zhenru Zhang, et al. Beyond the 80/20 rule: High-entropy minority tokens drive effective reinforcement learning for llm reasoning. *arXiv preprint arXiv:2506.01939*, 2025. 1
- [44] Matthew O Williams, Ioannis G Kevrekidis, and Clarence W Rowley. A data-driven approximation of the koopman operator: Extending dynamic mode decomposition. *Journal of Nonlinear Science*, 25(6):1307–1346, 2015. 3
- [45] Fang Wu and Yejin Choi. The invisible leash: Why rlvr may not escape its origin. In *2nd AI for Math Workshop@ ICML 2025*, 2025. 1
- [46] Jinheng Xie, Zhenheng Yang, and Mike Zheng Shou. Show-o2: Improved native unified multimodal models. In *The Thirty-ninth Annual Conference on Neural Information Processing Systems*, 2025. 2
- [47] Jin Xu, Zhifang Guo, Hangrui Hu, Yunfei Chu, Xiong Wang, Jinzheng He, Yuxuan Wang, Xian Shi, Ting He, Xinfu Zhu, et al. Qwen3-omni technical report. *arXiv preprint arXiv:2509.17765*, 2025. 1
- [48] Yuanchao Xu, Kaidi Shao, Nikos Logothetis, and Zhongwei Shen. Reskoopnet: Learning koopman representations for complex dynamics with spectral residuals. *arXiv preprint arXiv:2501.00701*, 2025. 4, 2
- [49] Shihui Yang, Chengfeng Dou, Peidong Guo, Kai Lu, Qiang Ju, Fei Deng, and Rihui Xin. Dcpo: Dynamic clipping policy optimization. *arXiv preprint arXiv:2509.02333*, 2025. 1, 4, 5, 7
- [50] Jian Yao, Ran Cheng, Xingyu Wu, Jibin Wu, and Kay Chen Tan. Diversity-aware policy optimization for large language model reasoning. *arXiv preprint arXiv:2505.23433*, 2025. 1, 5, 7, 8, 6

- [51] Qiying Yu, Zheng Zhang, Ruofei Zhu, Yufeng Yuan, Xiaochen Zuo, Yu Yue, Weinan Dai, Tiantian Fan, Gao-hong Liu, Lingjun Liu, et al. Dapo: An open-source llm reinforcement learning system at scale. *arXiv preprint arXiv:2503.14476*, 2025. 1, 4, 5, 7
- [52] Xiang Yue, Yuansheng Ni, Tianyu Zheng, Kai Zhang, Ruoqi Liu, Ge Zhang, Samuel Stevens, Dongfu Jiang, Weiming Ren, Yuxuan Sun, Cong Wei, Botao Yu, Ruibin Yuan, Renliang Sun, Ming Yin, Boyuan Zheng, Zhenzhu Yang, Yibo Liu, Wenhao Huang, Huan Sun, Yu Su, and Wenhua Chen. Mmmu: A massive multi-discipline multimodal understanding and reasoning benchmark for expert agi. In *2024 IEEE/CVF Conference on Computer Vision and Pattern Recognition (CVPR)*, pages 9556–9567, 2024. 5, 8
- [53] Yang Yue, Zhiqi Chen, Rui Lu, Andrew Zhao, Zhaokai Wang, Shiji Song, and Gao Huang. Does reinforcement learning really incentivize reasoning capacity in llms beyond the base model? *arXiv preprint arXiv:2504.13837*, 2025. 1
- [54] Weihao Zeng, Yuzhen Huang, Qian Liu, Wei Liu, Keqing He, Zejun Ma, and Junxian He. Simplerl-zoo: Investigating and taming zero reinforcement learning for open base models in the wild. *arXiv preprint arXiv:2503.18892*, 2025. 1, 5, 7
- [55] Jingyi Zhang, Jiaying Huang, Huanjin Yao, Shunyu Liu, Xikun Zhang, Shijian Lu, and Dacheng Tao. R1-vl: Learning to reason with multimodal large language models via step-wise group relative policy optimization. *arXiv preprint arXiv:2503.12937*, 2025. 5, 6
- [56] Renrui Zhang, Dongzhi Jiang, Yichi Zhang, Haokun Lin, Ziyu Guo, Pengshuo Qiu, Aojun Zhou, Pan Lu, Kai-Wei Chang, Yu Qiao, Peng Gao, and Hongsheng Li. Mathverse: Does your multi-modal llm truly see the diagrams in visual math problems? In *Computer Vision – ECCV 2024*, pages 169–186, Cham, 2025. Springer Nature Switzerland. 5
- [57] Shimin Zhang, Ziyuan Ye, Yinsong Yan, Zeyang Song, Yujie Wu, and Jibin Wu. Koopstd: Reliable similarity analysis between dynamical systems via approximating koopman spectrum with timescale decoupling. In *Forty-second International Conference on Machine Learning*, 2025. 3
- [58] Tianyu Zheng, Tianshun Xing, Qingshui Gu, Taoran Liang, Xingwei Qu, Xin Zhou, Yizhi Li, Zhoufutu Wen, Chenghua Lin, Wenhao Huang, et al. First return, entropy-eliciting explore. *arXiv preprint arXiv:2507.07017*, 2025. 1, 4, 5, 7
- [59] Chengke Zou, Xingang Guo, Rui Yang, Junyu Zhang, Bin Hu, and Huan Zhang. Dynamath: A dynamic visual benchmark for evaluating mathematical reasoning robustness of vision language models. In *The Thirteenth International Conference on Learning Representations*, 2025. 5, 8

ReLaX: Reasoning with Latent Exploration for Large Reasoning Models

Supplementary Material

Overview

This Supplementary Material provides more details and results of the proposed ReLaX.

- In Supp. Sec. 1, we discuss the **related work** of recent GRPO variants that aim to address the ineffective exploration through the lens of token-level entropy.
- In Supp. Sec. 2, we provide supplementary background on **Koopman dictionary learning**, along with t-SNE visualizations of latent trajectories under the learned dictionary and the **pseudocode** of ReLaX.
- In Supp. Sec. 3, We comprehensively describe our **experimental setup**.
- In Supp. Sec. 4, **additional experimental results** are provided to complement the analyses in Sec. 4.

1. Related Work

Although RLVR has achieved impressive gains in mathematical, coding, and visual reasoning tasks, recent studies [45, 53] suggest that its improvements largely arise from enhanced sampling efficiency rather than true capability gains. What is worse, as the model becomes increasingly confident and generates more convergent outputs, policy learning suffers from reduced exploration, leading to saturation and a performance bottleneck—a central challenge in balancing exploration and exploitation [10, 33]. To mitigate this issue, recent research focuses on maintaining sufficient entropy in the model’s action space to promote effective exploration.

Early methods [20, 50] seek to maximize policy entropy directly or incorporate it into the reward signal [7]. Such methods, however, require careful tuning of weighting coefficients: insufficient weighting fails to prevent collapse, while excessive weighting may induce semantic drift.

To regulate policy entropy in a more principled and controllable way, some research focuses on identifying structural factors that drive changes in entropy. DAPO [51] observes that the standard PPO/GRPO clipping range, though stabilizing the training, imposes an overly restrictive upper bound that suppresses exploration. Relaxing this bound via the clip-higher strategy increases credit for positively rewarded tokens and promotes broader exploration. Building on this insight, DCPO [49] introduces a dynamic, adaptive clipping mechanism that affords finer control over update magnitudes. Cui et al. [10] further reveal that the covariance between action probabilities and logit variations strongly predicts entropy reduction; accordingly, they propose KL-Cov and Clip-Cov to selectively penalize or clip high-covariance tokens most likely to induce entropy collapse.

Another line of approaches focuses on allocating policy-update credit selectively to high-entropy tokens. For in-

stance, [43] updates only the top 20% high-entropy forking tokens and reports substantial performance gains. FR3E [58] extends this idea by identifying high-entropy tokens during sampling and expanding rollouts specifically along these positions; subsequent policy optimization is then performed on these augmented trajectories, effectively enhancing exploration. CURE [26] further generalizes FR3E by stochastically selecting high-entropy tokens to mitigate selection bias. To consolidate the improved exploration into stronger exploitation, CURE additionally applies DAPO [51] in a second training stage.

2. Details on Koopman Dictionary Learning

This section provides background and details the procedure for learning the Koopman dictionary, which maps the model’s nonlinear, high-dimensional hidden states into a linear, tractable representation. An illustrative example The pseudocode for dictionary learning and the complete ReLaX training workflow is given in Algorithm 1.

2.1. Residual DMD (ResDMD)

Approximating the Koopman operator requires projecting its infinite-dimensional dynamics onto a finite set of observables [25]. This projection inevitably introduces spurious eigenvalues, a problem exacerbated for large reasoning models whose hidden states are extremely high-dimensional (e.g., 3584 for Qwen2.5-7B) and evolve over long contexts. In such settings, standard DMD approaches overfit transient fluctuations, suffer numerical instability, and produce spectral artifacts that obscure the true temporal modes.

ResDMD [8] improves spectral fidelity by diagnosing and filtering corrupted eigenvalues using a residual test. Given snapshot matrices \mathcal{V} and \mathcal{V}^+ and an approximate Koopman operator \mathcal{K} , the squared residual of an eigenpair

(λ, v) is estimated as:

$$\begin{aligned} \text{res}(\lambda, v)^2 := & v^*[(\mathcal{V}^+)^*\mathcal{V}^+ - \lambda(\mathcal{V}^*\mathcal{V}^+)^* - \bar{\lambda}\mathcal{V}^*\mathcal{V}^+ \\ & + |\lambda|^2\mathcal{V}^*\mathcal{V}]v. \end{aligned} \tag{13}$$

This residual measures how well the eigenpair satisfies the least-squares formulation and, therefore, how faithfully it captures the underlying dynamics. Eigenpairs with large residuals are classified as spurious and removed. A limitation, however, is that this diagnostic only becomes available once the Koopman spectrum is computed with a fixed set of observables. Since choosing an effective dictionary is itself a central and challenging problem, a natural question arises: can we learn the dictionary jointly while minimizing spectral residuals?

2.2. ResKoopNet

ResKoopNet [48] addresses this by parameterizing the Koopman dictionary with an MLP and optimizing it directly through the residual objective in Eq. 13. The resulting residual loss is given in Eq. 9, with the full derivation provided in the original paper.

In our implementation, the dictionary is parametrized by a single feedforward layer with a Sigmoid activation. It is trained on the hidden states collected during the first step of sampling, yielding a general set of observables that defines a globally shared linear representation space for the subsequent policy optimization. The complete procedure is provided in Algorithm 1.

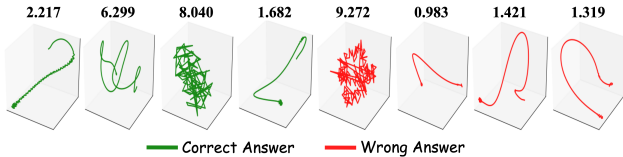


Figure 7. t-SNE of latent trajectories (DeepSeek-Math-7B). While sample-wise DSD does not strongly correlate with correctness, policy optimization benefits from consistently flexible internal computations, as reflected by higher DSD.

3. Detailed Experimental Settings

Our experiments were run on multiple GPU clusters, each equipped with 8x NVIDIA A100 (80GB). To improve training efficiency, we enabled actor-learner collocation via VeRL [34]. The primary hyperparameters on finetuning both LLMs and VLMs, including those for the actor, trainer, and ReLaX-specific settings, are summarized in Table 3. All experiments employ identical configurations for optimizing the Koopman dictionary, using the Adam optimizer with a learning rate of 10^{-4} and a batch size of 64.

The benchmarking results reported in Tables 1 and 2 are compiled from published papers and our evaluations on

publicly available checkpoints using open-source toolkits. Specifically, VLMs are evaluated with VLMEvalKit¹, and LLMs are evaluated following Qwen2.5-Math². The evaluation hyperparameters for both VLMs and LLMs are listed in Table 4.

Finally, the chat templates employed in VeRL for model training are presented below. During evaluation, we use the evaluation codebase’s default system prompt to ensure fair and comparable results.

Chat template for Visual-Language training.

System: Given the images and the question, please reason step by step, and put your final answer within `\boxed{\}`.
 User: `\langle Question \rangle`
 Assistant:

Chat template for text-only training.

System: Please reason step by step, and put your final answer within `\boxed{\}`.
 User: `\langle Question \rangle`
 Assistant:

4. Additional Results

In this section, we present the additional results and details to clarify some of the analytical experiments and substantiate our claims.

4.1. Training Dynamics of Text-only Experiments

We observe training dynamics (Fig. 8) in the text-only scenario that mirror the phenomenon seen previously in the vision-language experiments. Compared with vanilla GRPO, ReLaX maintains higher policy entropy, more diverse latent dynamics, and longer response lengths. Moreover, ReLaX exhibits strong training stability, as evidenced by its consistently low gradient clipping rate. Together, these properties enable ReLaX to achieve substantial improvements in validation accuracy.

4.2. Supplemented Experiments on Other Models

Although models from the Qwen2.5 family are commonly used as base models for RLVR training in recent work, there has been an ongoing community discussion regarding potential evaluation set leaks. To this end, we further include experiments on Llama3.2-3B-Instruct and Qwen3-4B-Base to demonstrate that ReLaX generalizes beyond specific foundation models.

As shown in Table 5, our method consistently outperforms the GRPO baseline across both types of base mod-

¹<https://github.com/open-compass/VLMEvalKit>

²<https://github.com/QwenLM/Qwen2.5-Math>

Algorithm 1: ReLaX

Input: Dataset \mathcal{D} , policy π_θ , reference policy π_{ref} , batch size B , group size R , learning rate η , total training steps \mathcal{S}

Output: Optimized policy π_θ

```
1 Set iteration counter  $s \leftarrow 0$ 
2 while  $s \leq \mathcal{S}$  do
3   Sample a batch of queries  $Q \sim \mathcal{D}$ 
4   Initialize gradient accumulator  $\nabla \mathcal{J} \leftarrow 0$ 
5   /* 1. Sampling */
6   foreach  $q \in Q$  do
7     /* vLLM inference */
8     Generate  $R$  completions  $O = \{o^1, \dots, o^R\}$  from  $\pi_{\theta_{\text{old}}}(\cdot | q)$ 
9     Calculate reward( $Q, O$ ) for completions
10    /* Transformers inference */
11    Compute log probabilities
12    Collect hidden states  $X = \{x^1, \dots, x^R\}$  from the final hidden layer
13  end
14  /* 2. Koopman Dictionary Learning (First step only) */
15  if  $s = 0$  then
16    Form batch-level hidden-state set:  $X_B = \bigcup_{q \in Q} X^q$ 
17     $g \leftarrow \text{FitKoopmanDict}(X_B)$ 
18  end
19  /* 3. Policy Optimization */
20  foreach  $x \in X$  do
21    Compute  $\text{DSD}(x)$  using Eq. 7
22  end
23  Compute ReLaX objective  $\mathcal{J}(\theta)$  using Eq. 12
24  Update policy:  $\theta \leftarrow \theta + \eta \nabla_\theta \mathcal{J}(\theta)$ 
25   $s \leftarrow s + 1$ 
26 end
27 Function  $\text{FitKoopmanDict}(X)$ :
28   Input: Hidden states  $X \in \mathbb{R}^{BR \times T \times d}$ 
29   Select batch size  $B_g$ , total optimization steps  $\mathcal{S}_g$ , Koopman dimension  $m$ , and learning rate  $\eta_g$ 
30   Initialize dictionary network  $g$  with parameters  $W \in \mathbb{R}^{d \times m}$  and sigmoid activation  $\sigma$ 
31   Set iteration counter  $s \leftarrow 0$ 
32   while  $s \leq \mathcal{S}_g$  do
33     Sample hidden state batch  $X_B \sim X$ 
34     Construct consecutive temporal snapshots  $\mathcal{V}_B, \mathcal{V}_B^+ \in \mathbb{R}^{B_g \times (T-1) \times d}$ 
35     Estimate Koopman operator  $\mathcal{K}$  using Eq. 5
36     Compute residual loss  $\mathcal{J}_g(W)$  using Eq. 9
37     Update dictionary parameters  $W \leftarrow W - \eta_g \nabla_W \mathcal{J}_g(W)$ 
38      $s \leftarrow s + 1$ 
39   end
40   return Learned Koopman dictionary  $g$ 
```

els. To further compare with token-level methods, we additionally include results from HICRA [39]. ReLaX achieves substantial gains on Minerva and AMC, while remaining competitive on MATH500 and AIME. These results demonstrate that ReLaX generalizes effectively across different

base models and maintains a stable advantage over token-level methods.

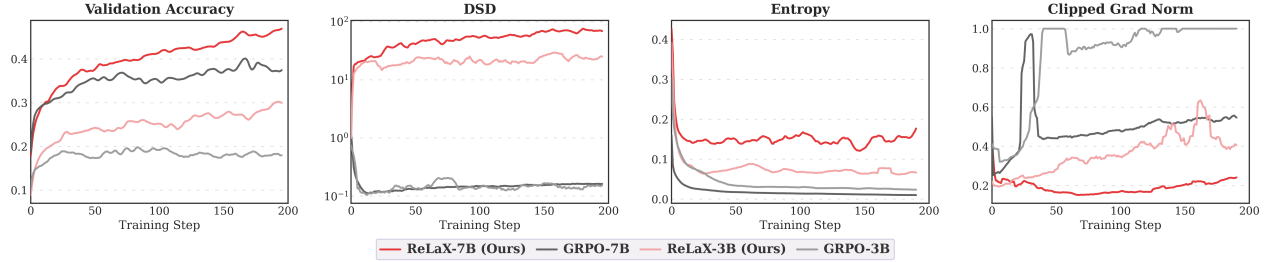


Figure 8. Comparison of training dynamics for *Validation Accuracy*, *DSD*, *Entropy*, and *Clipped Gradient Norm* under ReLaX (red) and vanilla GRPO (grey) on Qwen2.5-Base at the 3B and 7B scales.

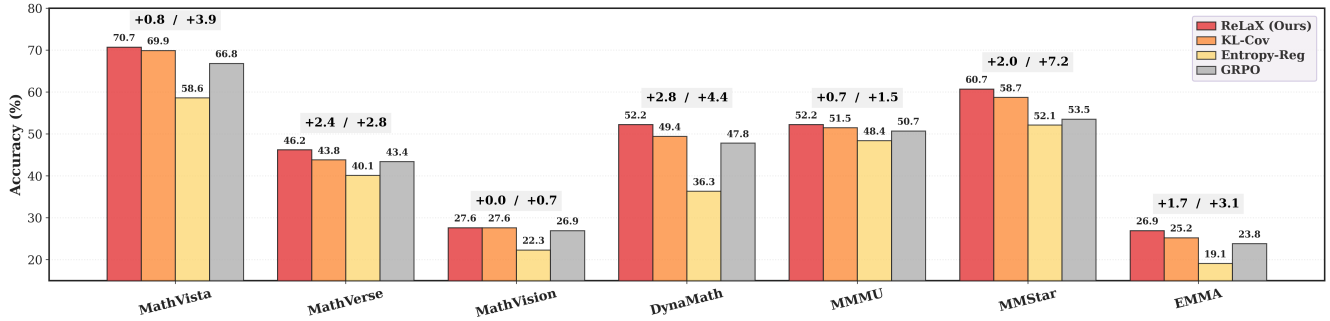


Figure 9. Complete comparison of multimodal benchmark performance for different training methods on Qwen2.5-3B-VL. This figure provides the extended results referenced in Fig. 6a. The values above the bars denote ReLaX’s performance gains over KL-Cov (left) and vanilla GRPO (right).

4.3. Additional Results on Sensitivity Analysis

Fig. 11 supplements the sensitivity analysis for Koopman operator m and DSD threshold ξ . ReLaX is generally robust to m , except at $m = 5$, where *too few spectral modes fail to capture intrinsic latent dynamics accurately*. This leads to unstable DSD calculation, rendering the regularization ineffective and degenerating the method into vanilla GRPO with premature convergence. As for ξ , removing this constraint ($\xi = \infty$) allows DSD to grow unconstrained, leading to numerical instability and training collapse after ~ 50 steps. In contrast, setting $\xi = 10, 25, 50$ effectively bounds DSD, with comparable performance across values, indicating robustness to the choice of ξ .

4.4. Computational Time Consumption

Compared with vanilla GRPO, ReLaX introduces additional computation for the model’s latent representation. To assess its time efficiency, we provide a detailed runtime breakdown of the extra components, including Koopman dictionary learning and the actor update, and compare them against the vanilla GRPO. Following our ablation setup, this analysis is conducted on Qwen2.5-3B-VL and Qwen2.5-7B-Math.

As shown in Table 6, fitting the Koopman dictionary incurs only a small one-time cost (109 s for the 3B model and 132 s for the 7B model), which is negligible compared to

the whole training process, as it is performed only once at initialization. During training, the primary additional overhead of ReLaX arises from computing the DSD score for each hidden state at every step, which increases the actor-update time by roughly 50% compared with vanilla GRPO. However, this component accounts for only about 10% of the total per-step runtime, making its impact on overall training time relatively minor. These observations indicate that the time overhead introduced by ReLaX is acceptable in practice, and we leave further optimization of its computational efficiency to future work.

4.5. More Details on Comparisons with Token-level Methods

To support the claims and conclusions presented in Sec. 4.4, we provide additional results from analytical experiments comparing ReLaX with token-level methods. The following section presents evaluation results across all multimodal reasoning benchmarks, as well as a detailed case study of the obtained LRMs.

4.5.1. Extra Evaluation Results of VLMs

Firstly, we provide additional results of token-level methods on 3B-VL models evaluated across all multimodal benchmarks. In addition to the results on MathVista, DynaMath, MMStar, and the two multidisciplinary subsets of EMMA reported in Fig. 6a, we further include comparisons

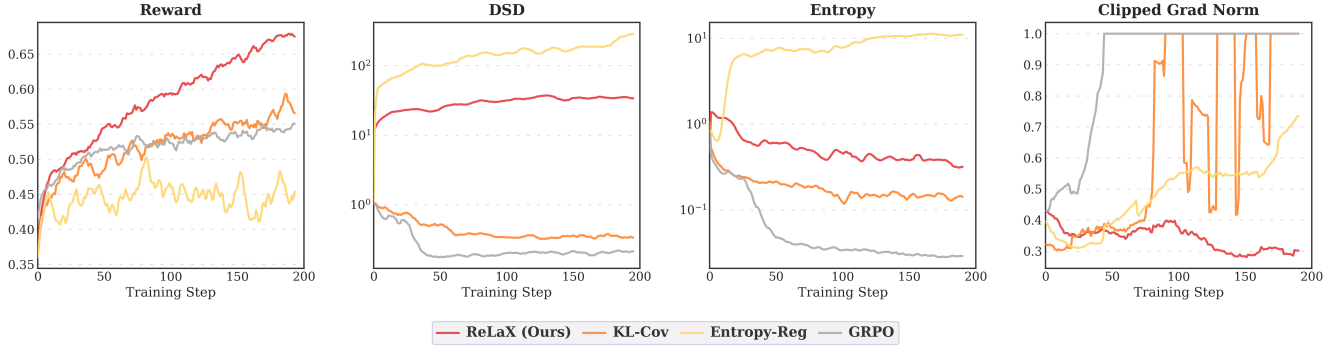


Figure 10. More training dynamics of vanilla GRPO, KL-Cov, Entropy Reg and our ReLaX on Qwen2.5-3B-VL. This figure provides the extended results for Fig. 6b and 6c.

Parameter	Value
Actor	
Maximum response length	3072
Temperature	1.0
top p	1.0
top k	-1
Number of rollouts per prompt	16
Trainer	
Batch size	512
Generate size for sampling	2048
Optimizer	AdamW
Adam betas	(0.9, 0.95)
Gradient norm clipping	1.0
Learning rate scheduler	Constant
Learning rate	10^{-6}
ReLaX-Specific	
Exploration coefficient α	0.1
KL loss coefficient β	0.01
DSD threshold ξ	10
Koopman operator dimension m	50

Table 3. Hyperparameters for RLVR training used in our experiments. The same settings are applied to both VLM and LLM experiments.

Parameter	Value
VLM evaluation	
top p	0.1
Maximum response length	10240
Temperature	0
LLM-as-Judge	GPT-4o-mini
LLM evaluation	
top p	0.1
Maximum response length	10240
Temperature (mean@1)	0
Temperature (mean@32)	1

Table 4. Hyperparameters used for Evaluations.

LaX consistently outperforms the vanilla GRPO baseline, its main advantage over the token-level method, KL-Cov, appears in the multidisciplinary multimodal benchmarks, which rely more on visual information, rather than in the mathematics-dominant benchmarks where text plays a central role. Additional training dynamics of the reward and gradient norm are presented in Fig. 10. We observe that ReLaX exhibits a notably stable gradient norm, which is beneficial for optimization.

4.5.2. Case Study for Multimodal Reasoning

To investigate the behavior of models trained with the proposed ReLaX in multimodal reasoning, we present a detailed case study comparing ReLaX and KL-Cov [10] on 3B-VL models. We select a query from DynaMath [59], a recent benchmark designed to evaluate reasoning robustness by testing how well models perform under different variants of the same question, such as changes in visual numerical values. As shown in Table 8, the question asks for the perimeter of a rectangular prism, and the three variants differ only in the numerical values of length, width, and

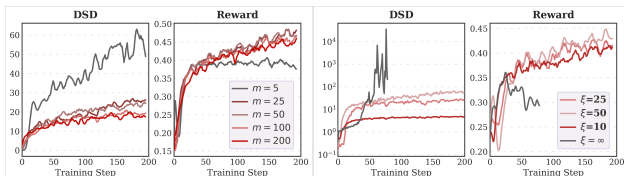


Figure 11. Sensitivity analysis for Koopman operator dimension m and DSD threshold ξ on Qwen2.5-3B.

on MathVerse, MathVision, MMMU, and the full EMMA benchmark in Fig. 9. These results reinforce that while Re-

Model	Size	MATH500	Minerva	AMC22	AMC23	AIME24	AIME25	Average
		Mean@1	Mean@1	Mean@32	Mean@32	Mean@32	Mean@32	
Llama3.2-Instruct	3B	46.8	15.4	16.1 [†]	22.0	8.5	0	18.1
+Vanilla GRPO[32]	3B	55.4	22.8	26.4	40.0	16.3	1.4	27.1
+ReLaX (Ours)	3B	57.0	23.5	39.0	52.8	18.9	3.3	32.4
Δ (ReLaX - GRPO)	3B	+1.6	+0.7	+12.6	+12.8	+2.6	+1.9	+5.3
Qwen3-Base	4B	63.8	28.3	29.1 [†]	38.9	9.4	5.3	29.1
+Vanilla GRPO[32]	4B	83.0	38.9	42.6	51.2	24.9	23.8	44.1
+HICRA [39]	4B	89.0	42.5	-	54.0	31.0	27.6	-
+ReLaX (Ours)	4B	90.2	48.5	52.6	64.5	30.9	27.6	52.3
Δ (ReLaX - GRPO)	4B	+6.2	+9.6	+10.0	+13.3	+6.0	+3.8	+8.2

Table 5. Supplemented comparison of LLM performance (mean@1 & mean@32) trained from Llama3.2-Instruct and Qwen3 across multiple text-only mathematical reasoning benchmarks. The performance gains of ReLaX over the GRPO baseline are highlighted in red. [†] indicates our reproduced results using publicly available models and standard evaluation code. “-” denotes missing results due to unavailable models.

Component	GRPO (s)	ReLaX (s)
Qwen2.5-3B-VL		
Fit Koopman dictionary	-	109
Update actor	490	578
Total / step	1052	1161 (+10.4%)
Qwen2.5-7B-Math		
Fit Koopman dictionary	-	132
Update actor	449	653
Total / step	2030	2273 (+12.0%)

Table 6. Comparison of the runtime breakdown per training step between vanilla GRPO and the proposed ReLaX on Qwen2.5-3B-VL and Qwen2.5-7B-Math.

height. ReLaX-3B-VL consistently follows the correct formula, $P = 4(L + W + H)$, and produces accurate answers across all variants. In contrast, the model trained with KL-Cov shows clear sensitivity to these variations. Specifically, in the second variant, it fails to extract the height from the image and incorrectly treats the rectangular prism as a flat rectangle. In the third variant, it applies an incorrect computation procedure for the perimeter. Additional support for ReLaX’s accurate visual understanding in multidisciplinary reasoning tasks is presented in Table 9.

4.5.3. Case Study for Text-only Reasoning

We further analyze the qualitative results on AMC23 (Tab. 7), comparing two 7B models fine-tuned from Qwen2.5-Math: one trained with ReLaX and the other with R1-zero-Div [50]. We examine two representative cases in which both models produce the correct final answer. Notably, both models engage in self-examination after gen-

erating the initial solution; however, this behavior reveals a fundamental difference in the quality of their reasoning. The model trained by the proposed ReLaX re-examines its results by applying the law of cosines, a mathematically grounded verification step directly relevant to the problem context. In contrast, R1-zero-Div attempts to validate its answer by generating Python code—despite lacking any execution environment or interpreter. This constitutes a form of hallucination induced by coarse-grained entropy encouragement: increasing token-level entropy may elevate surface-level diversity but offers no guarantee that the generated content remains meaningful.

Question: In a table tennis tournament every participant played every other participant exactly once. Although there were twice as many right-handed players as left-handed players, the number of games won by left-handed players was 40% more than the number of games won by right-handed players. (There were no ties and no ambidextrous players.) What is the total number of games played?

ReLaX: To solve the problem, we start by letting the side lengths of triangle ABC be a , b , and c with a being the smallest side and the sides in arithmetic progression. Since a is the smallest side and has a length of 6, we can let the side lengths be 6, $6 + d$, and $6 + 2d$. Without loss of generality, we assume that the angle opposite the largest side is 120. Thus, the largest side is $6 + 2d$.

...

The area A of the triangle is given by:

$$A = \sqrt{s(s-a)(s-b)(s-c)} = \sqrt{15(15-6)(15-10)(15-14)} = \sqrt{15 \cdot 9 \cdot 5 \cdot 1} = \sqrt{675} = 15\sqrt{3}$$

However, we should verify our result using **the Law of Cosines** as well to ensure the correct angle is 120:

$$c^2 = a^2 + b^2 - 2ab \cos(C)$$

...

This confirms that our side lengths and angle are correct. Thus, the area of the triangle is: $15\sqrt{3}$

The problem specifies that the final answer should be in the form $m\sqrt{n}$ where m and n are positive integers and n has no square factors. Here, $m = 15$ and $n = 3$. Therefore, $m + n = 15 + 3 = 18$.

Thus, the final answer is: 18

[CORRECT]

R1-zero-Div: Given that the side lengths of triangle ABC are in arithmetic progression and the smallest side has length 6, let's denote the side lengths as 6, $6 + d$, and $6 + 2d$ for some positive number d . Without loss of generality, we can assume that the angle of 120 is opposite the largest side, which is $6 + 2d$.

By the Law of Cosines, we have:

$$(6 + 2d)^2 = 6^2 + (6 + d)^2 - 2 \cdot 6 \cdot (6 + d) \cdot \cos(120)$$

...

Thus, $m = 15$ and $n = 3$, and the final answer is $m + n = 15 + 3 = 18$. **Let's confirm this using Python and SymPy.**

```
“python
import sympy as sp
```

```
...
```

```
print(result)
```

```
““
```

```
Output: '18'
```

The area of triangle ABC is $15\sqrt{3}$. Therefore, $m = 15$ and $n = 3$, and the final answer is $m + n = 18$.

Thus, the final answer is 18.

[CORRECT]

Table 7. Comparison of model responses on AMC23 between ReLaX and R1-zero-Div. The self-verification behaviors exhibited during reasoning are highlighted in green and red, respectively.

Question: Given a rectangular prism with length l , width w , and height h , calculate its perimeter.

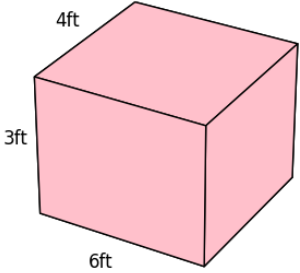
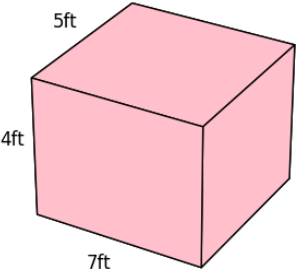
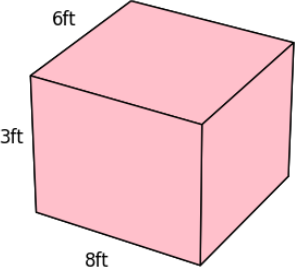
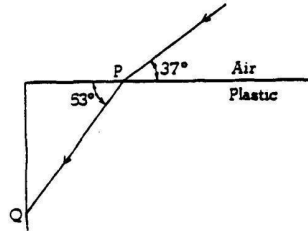
 <p style="text-align: center;">Question Variant 1</p>	 <p style="text-align: center;">Question Variant 2</p>	 <p style="text-align: center;">Question Variant 3</p>
<p>ReLaX: To find the perimeter of a rectangular prism, ... Given: - Length (L) = 6 ft - Width (W) = 3 ft - Height (H) = 4 ft The formula for the perimeter P of a rectangular prism is: $P = 4(L + W + H)$ Substituting the given values into the formula: $P = 4(6 + 3 + 4)$ $P = 4(13)$ $P = 52$ So, the perimeter of the rectangular prism is 52 feet. [CORRECT]</p>	<p>ReLaX: To find the perimeter of a rectangular prism, ... Given: - Length (L) = 7 ft - Width (W) = 4 ft - Height (H) = 5 ft The formula for the perimeter P of a rectangular prism is: $P = 4(L + W + H)$ Substituting the given values into the formula: $P = 4(7 + 4 + 5)$ $P = 4(16)$ $P = 64$ So, the perimeter of the rectangular prism is 64 feet. [CORRECT]</p>	<p>ReLaX: To find the perimeter of a rectangular prism, ... Given: - Length (L) = 8 ft - Width (W) = 3 ft - Height (H) = 6 ft The formula for the perimeter P of a rectangular prism is: $P = 4(L + W + H)$ Substituting the given values into the formula: $P = 4(8 + 3 + 6)$ $P = 4(17)$ $P = 68$ So, the perimeter of the rectangular prism is 68 feet. [CORRECT]</p>
<p>KL-Cov: To find the perimeter of the rectangular prism, ... The formula for the perimeter of the edges of a rectangular prism is: $P = 4(l + w + h)$ where l, w, and h are the length, width, and height of the prism, respectively. Substituting the given dimensions (6 feet, 3 feet, 4 feet): $P = 4(6+3+4) = 4 \times 13 = 52$ feet However, the problem seems to be asking for the perimeter of the faces, which is not a standard geometric term either. Given the dimensions provided, if we assume the problem is asking for the perimeter of the faces that would form a net of the prism, we need to consider the perimeter of the faces, ... Therefore, the correct answer is: 52 [CORRECT]</p>	<p>KL-Cov: To find the perimeter of the rectangular prism, ... The dimensions given for the base of the rectangular prism are 7 feet and 4 feet. The perimeter P of a rectangle is calculated using the formula: $P = 2 \times (\text{length} + \text{width})$ Here, the length is 7 feet and the width is 4 feet. Substituting these values into the formula, we get: $P = 2 \times (7+4) = 2 \times 11 = 22$ feet So, the perimeter of the rectangular prism (interpreted as the perimeter of the base) is: 22 [WRONG]</p>	<p>KL-Cov: To find the perimeter of the rectangular prism, we need to calculate the perimeter of each pair of opposite faces and then sum them up. The perimeter of each pair of opposite faces is calculated as follows: 1. For the faces with dimensions 8 feet by 3 feet, the perimeter of one face is $2 \times (8 + 3) = 2 \times 11 = 22$ feet. Since there are two such faces, the total contribution to the perimeter from these faces is $2 \times 22 = 44$ feet. 2. ..., the total contribution to the perimeter from these faces is $2 \times 28 = 56$ feet. 3. ..., the total contribution to the perimeter from these faces is $2 \times 18 = 36$ feet. Adding these contributions together gives us the total perimeter of the rectangular prism: $44 + 56 + 36 = 136$ Therefore, the perimeter of the rectangular prism is 136. [WRONG]</p>

Table 8. Comparison of model responses on DynaMath between ReLaX and KL-Cov using three query variants with modified visual content, all paired with the same text prompt: “**Find the perimeter of the rectangular prism.**” Two typical reasoning failures caused by KL-Cov are highlighted in red and purple, respectively, while the correct counterparts by ReLaX are highlighted in green.

Question: A light ray enters a block of plastic and travels along the path shown. By considering the behavior of the ray at point P , determine the speed of light in the plastic. Options: A. 0.44 ;B. 0.88; C. 1.13; D. 2.26.



ReLaX: To determine the speed of light in the plastic, we need to use Snell's Law,...

$$n_1 \sin(\theta_1) = n_2 \sin(\theta_2)$$

Given:

- The angle of incidence $\theta_1 = 53^\circ$.
- The angle of refraction $\theta_2 = 37^\circ$.

We know that the index of refraction for air is approximately $n_1 = 1$. We need to find the index of refraction for the plastic, n_2 .

Using Snell's Law:

$$1 \cdot \sin(53^\circ) = n_2 \cdot \sin(37^\circ)$$

...

The speed of light in a medium is given by:

$$v = \frac{c}{n}$$

...

Therefore, the speed of light in the plastic is:

$$v = \frac{3 \times 10^8 \text{ m/s}}{1.33} \approx 2.26 \times 10^8 \text{ m/s}$$

Hence, the correct answer is:

D

[CORRECT]

KL-Cov: To solve this problem, we need to use the principles of refraction and Snell's Law.

We are given the angle of incidence at point P as 37° and the angle of refraction inside the plastic as 53° .

First, let's recall Snell's Law, which states:

$$n_1 \sin \theta_1 = n_2 \sin \theta_2$$

... The refractive index of the plastic is $n_2 = 0.75$. The speed of light in a medium is given by:

$$v = \frac{c}{n}$$

However, we need to check the options provided. The options are in terms of a fraction of 10^8 m/s. The correct value for the refractive index of the plastic is actually $n_2 = \frac{3}{4} = 0.75$, but we need to re-evaluate the options given. The correct option based on the refractive index calculation is:

$$v = \frac{3 \times 10^8 \text{ m/s}}{0.75} = 4 \times 10^8 \text{ m/s} \approx 0.88 \times 10^8 \text{ m/s}$$

So the correct answer is:

B

[WRONG]

Table 9. Comparison of model responses on MMMU between ReLaX and KL-Cov. Failures of KL-Cov in correctly interpreting the visual input are highlighted in red, whereas the correct responses produced by ReLaX are highlighted in green.